Supporting Information

Cascade Reaction Mediated Efficient Ferroptosis Synergizes with Immunomodulation for High-performance Cancer Therapy

Authors: Zhaowei Li[a,b], Long Rong[a,b*]

Affiliations:

[a] Key Laboratory for Biomechanics and Mechanobiology of Ministry of Education, School of Biological Science and Medical Engineering, Beihang University, Beijing 100083, China

[b] Beijing Advanced Innovation Centre for Biomedical Engineering, Beihang University, Beijing 100083, China

* Corresponding author. Email: ronglong@buaa.edu.cn

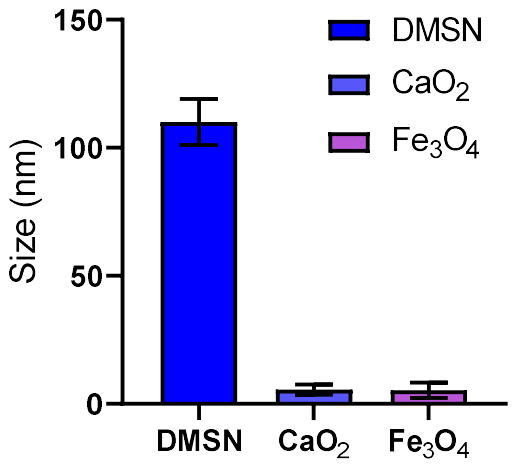

Figure S1. The particle sizes of DMSN, CaO_2, and Fe_3O_4. Data are represented as mean ± SD (n = 3). Results demonstrated that the sizes of DMSN, CaO_2, and Fe_3O_4 were about 110 nm, 5 nm, and 5 nm, respectively.

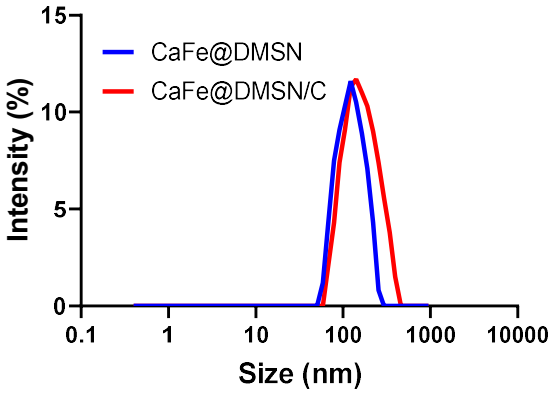

Figure S2. The hydrodynamic diameters of CaFe@DMSN and CaFe@DMSN/C measured by DLS. Results demonstrated that the size of CaFe@DMSN/C was slightly larger than CaFe@DMSN, indicating the successful coating of the membrane.

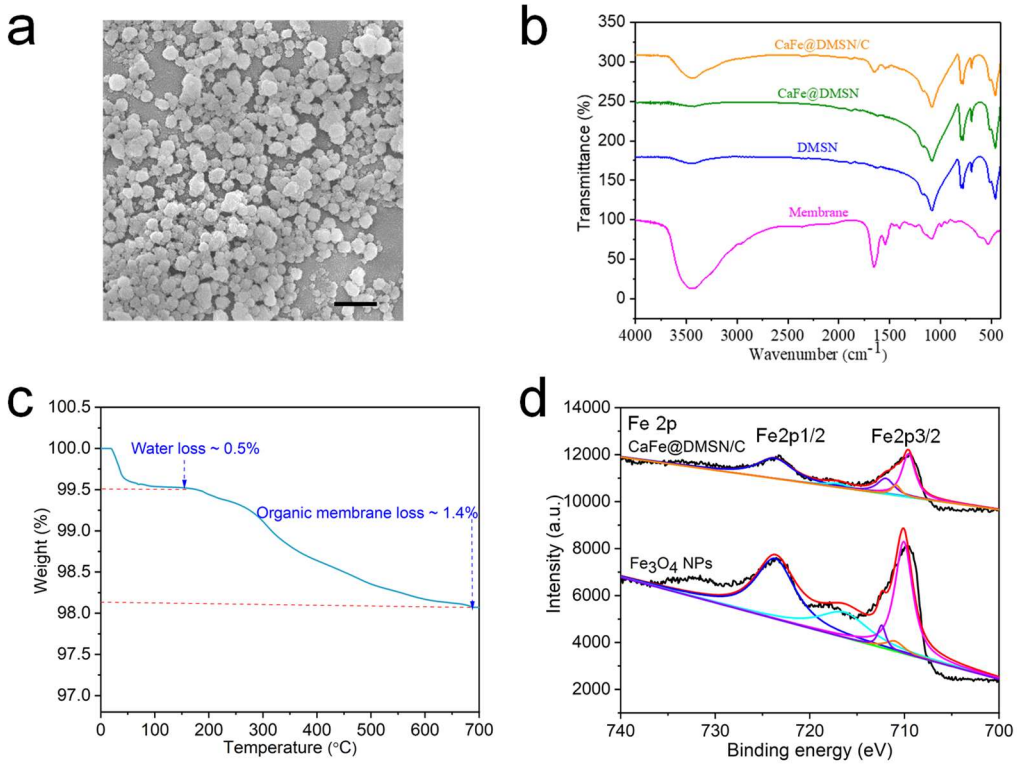

Figure S3. Characterization of the nanoformulations.

(a) Representative scanning electron microscope (SEM) image of CaFe@DMSN/C (scale bar: 20 nm). As shown in the image, CaFe@DMSN/C was uniformly dispersed with an average size of around 110 nm.

(b) FTIR spectroscopy analysis of the membrane, DMSN, CaFe@DMSN, and CaFe@DMSN/C. The peak at 1086.7 cm^{-1} (stretching vibration of the Si-O bond) indicated the successful preparation of the DMSN carrier. Moreover, the characteristic peak at 1500-1600 cm^{-1} (stretching vibration of the C=O bond) demonstrated the successful coating of the membrane.

(c) TG-DSC analysis of CaFe@DMSN/C. Results indicated that the organic components (membrane) contributed around 1.4 wt.% of the CaFe@DMSN/C, while the content of inorganic components was 98 wt.% and the remaining 0.5 wt.% was water.

(d) X-ray photoelectron spectroscopy (XPS) spectra of Fe_3O_4 and CaFe@DMSN/C. By comparing the characteristic peaks of Fe_3O_4 with the peaks in CaFe@DMSN/C, we confirmed that the oxidation state of iron in CaFe@DMSN/C was positive bivalent and trivalent. Notably, the peak at 709.5 eV was attributed to Fe^{2+}, while the peaks at 711.8 and 712.9 eV were caused by Fe^{3+}.

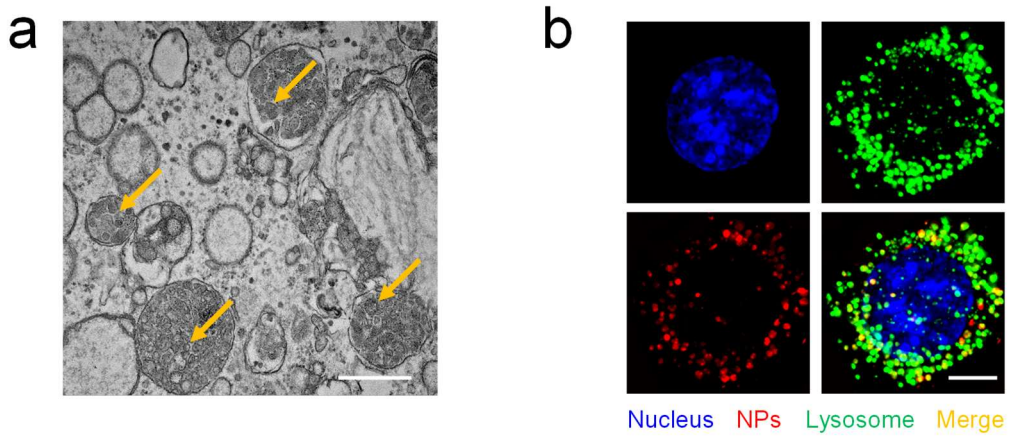

Figure S4. Cell uptake analysis of the nanoparticles after being endocytosed.
(a) Bio-TEM image of 4T1 cell (yellow arrow: nanoparticles; scale bar 500 nm).
(b) Representative confocal laser scanning microscope (CLSM) images and analysis of the nanoparticles co-localized with lysosomes after endocytosis (green: lysosome; blue: nucleus; red: nanoparticles; scale bar 5 μm).
These results together indicated that the nanoparticles mainly entered lysosomes after being endocytosed into tumor cells.

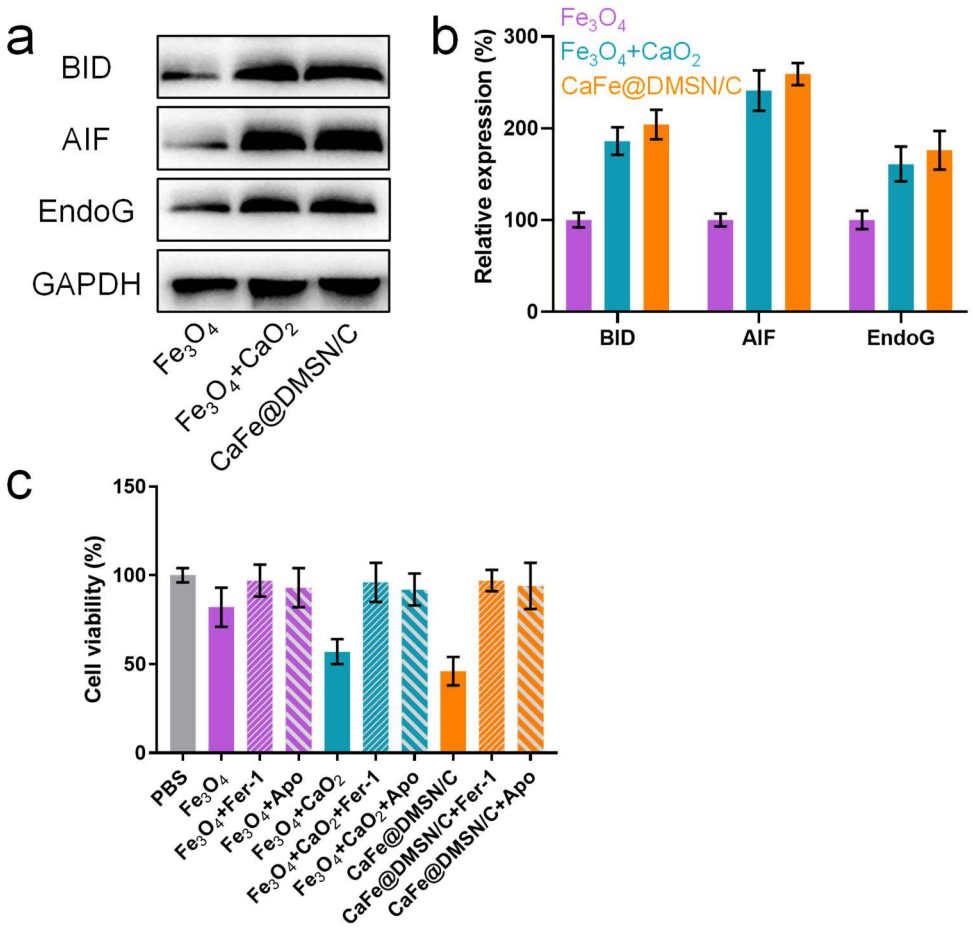

Figure S5. Evaluation on ferroptosis-induced tumor therapy.

(a b) Western blot and corresponding quantification analysis on the expression of key ferroptosis makers including BID, AIF, and EndoG. Results demonstrated that the expression of BID, AIF, and EndoG in cells treated by CaFe@DMSN/C increased by 2-, 2.5-, and 1.7-fold, respectively, compared with the Fe_3O_4 treatment group, strongly suggesting that the CaFe@DMSN/C could induce efficient ferroptosis.

(c) Cell viability analysis of 4T1 cells receiving different treatments. As the data shown, Fe_3O_4, Fe_3O_4+CaO_2 and CaFe@DMSN/C could exert anti-tumor effect. Notably, when they were combined with Fer-1 or Apo, the cell viability increased significantly, immediately suggesting that the prepared formulations exerted anti-tumor effect through ferroptosis.

Data are represented as mean ± SD (n = 3).

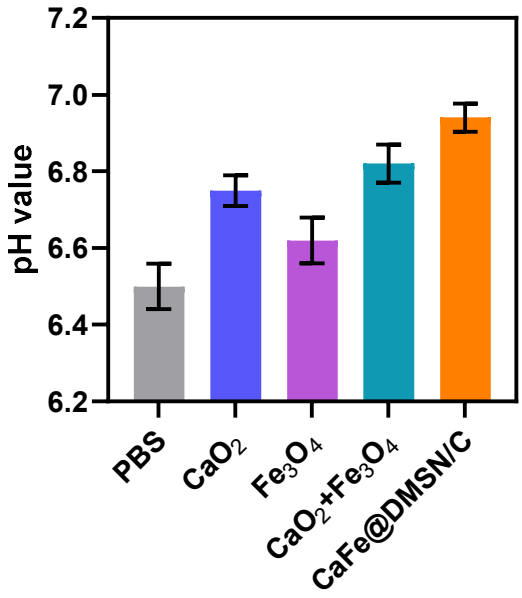

Figure S6. The pH changes *in vitro* in different treatment groups. Data are represented as mean ± SD (n = 3). The CaFe@DMSN/C could effectively modulate the pH value.

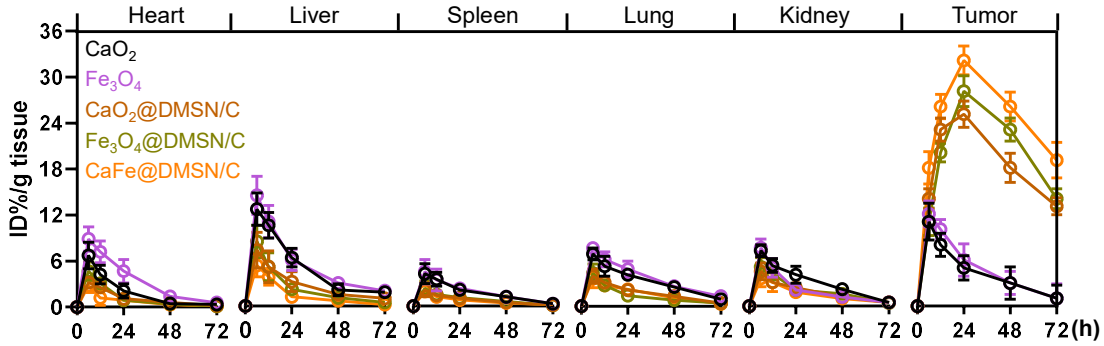

Figure S7. Biodistribution of different formulations in tumors and major organs at different time points post injection. Results demonstrated that CaO_2 and Fe_3O_4 distributed widely in tumors and major organs, indicating the potential off-target induced side effects. Notably, when they were loaded on the DMSN carrier and camouflaged with a membrane, the tumor accumulation increased significantly. Meanwhile, the distribution in normal organs decreased, reflecting the enhanced tumor targeting and the elimination of undesired side effects. Data are represented as mean ± SD (n = 6).

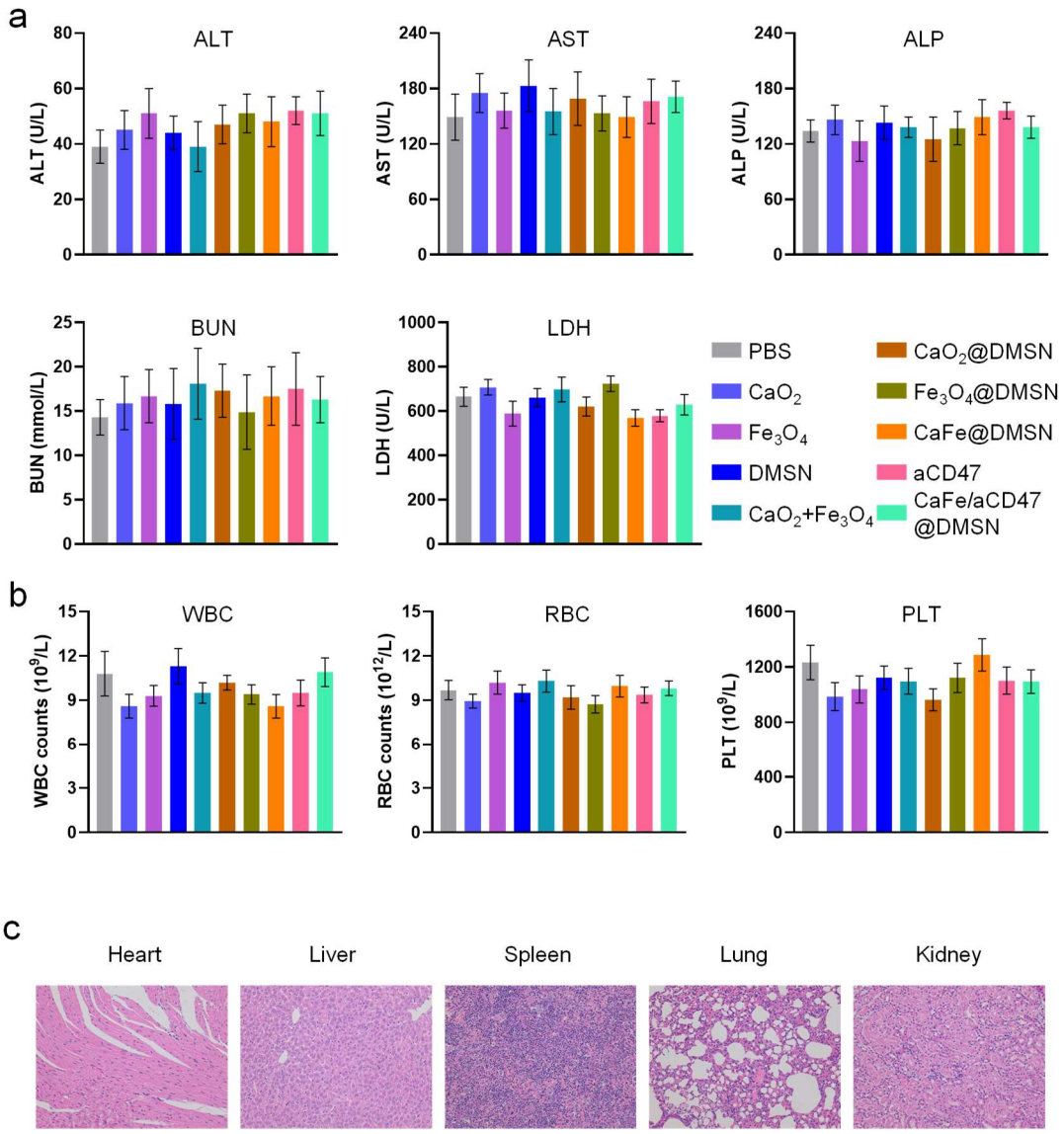

Figure S8. Safety evaluation of different formulations.

(a) Serum biochemical parameters detection.

(b) The blood routine examination.

(c) Representative histological examinations of H&E-stained organs from mice receiving CaFe@DMSN/C treatment.

Data are represented as mean ± SD (n = 6).

It can be observed from the analysis that all the prepared formulations exhibited good biocompatibility without abnormities.

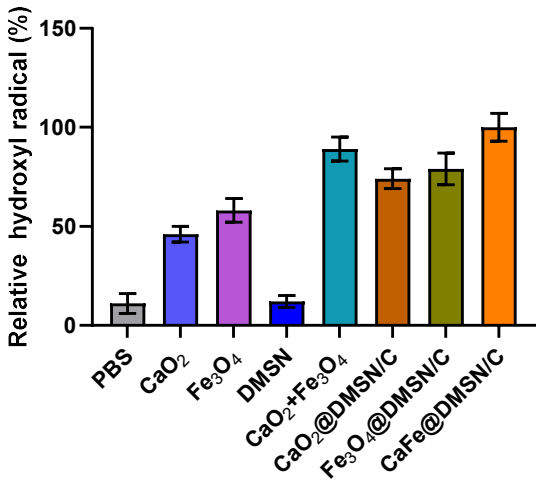

Figure S9. The production of hydroxyl radical in different treatment groups. Data are represented as mean ± SD (n = 6). The CaFe@DMSN/C exhibited excellent production ability of hydroxyl radical which well explained the potent anticancer performance.

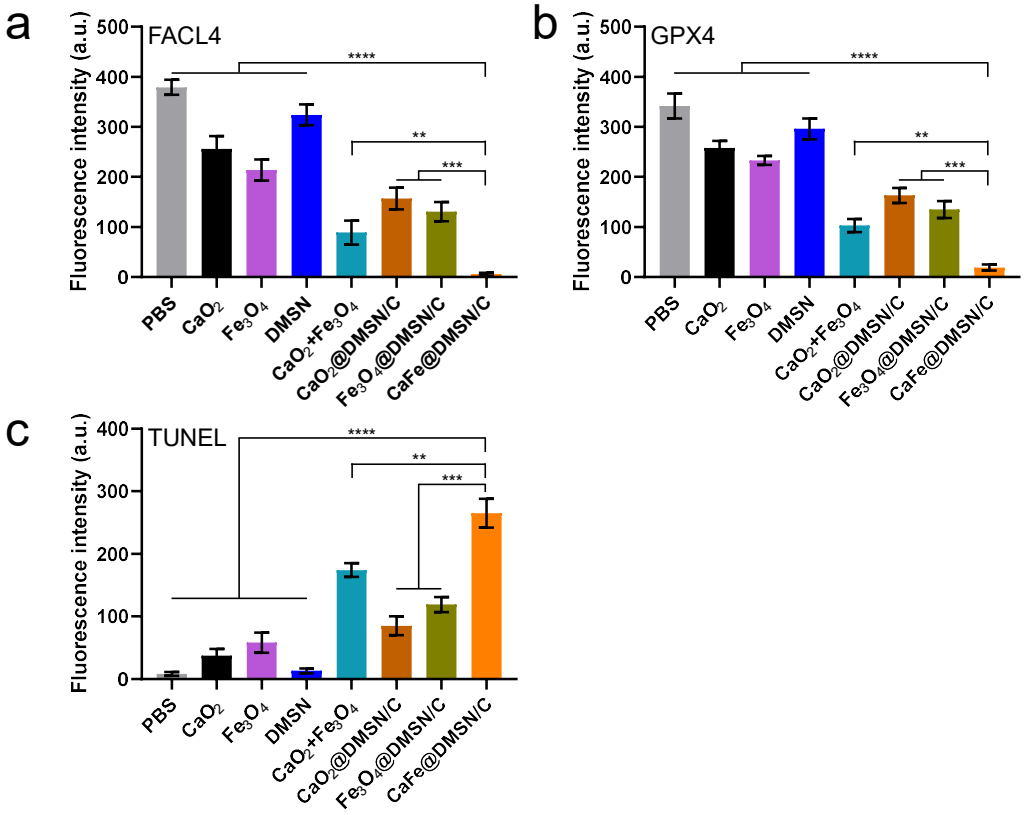

Figure S10. Corresponding quantification of the fluorescence intensity of FACL4 (a), GPX4 (b), and TUNEL (c) in tumor tissues receiving different treatments. ** $p<0.01$, *** $p<0.001$, **** $p<0.0001$. Data are represented as mean ± SD (n = 6).

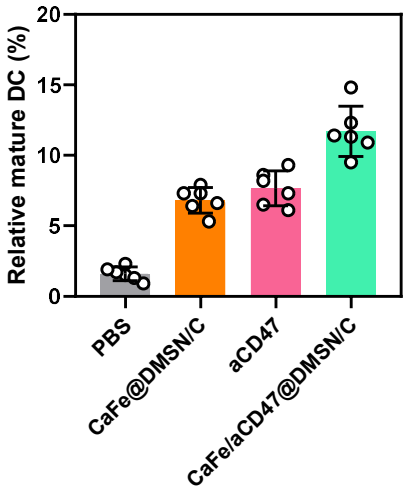

Figure S11. Relative mature DCs in primary tumors with different treatments on the resection day. The CaFe/aCD47@DMSN/C had the substantial improvement of the amount of mature DCs. Data are represented as mean ± SD (n = 6).